AGU PUBLICATIONS

JGR

Journal of Geophysical Research: Atmospheres

RESEARCH ARTICLE
10.1002/2014JD021947

Key Points:
- Evaporation and mixing control vapor isotope variability at the ocean surface
- Deuterium excess is a robust indicator of evaporative conditions over the ocean
- The water vapor residence time affects d-excess variability at the near surface

Correspondence to:
M. Benetti,
marion.benetti@locean-ipsl.upmc.fr

Citation:
Benetti, M., G. Aloisi, G. Reverdin, C. Risi, and G. Sèze (2015), Importance of boundary layer mixing for the isotopic composition of surface vapor over the subtropical North Atlantic Ocean, *J. Geophys. Res. Atmos.*, *120*, doi:10.1002/2014JD021947.

Received 28 APR 2014
Accepted 8 FEB 2015
Accepted article online 11 FEB 2015

Importance of boundary layer mixing for the isotopic composition of surface vapor over the subtropical North Atlantic Ocean

Marion Benetti[1], Giovanni Aloisi[1], Gilles Reverdin[1], Camille Risi[2], and Geneviève Sèze[2]

[1]Sorbonne Universités (UPMC, University of Paris 06)-CNRS-IRD-MNHN, LOCEAN, Paris, France, [2]Laboratoire de Météorologie Dynamique, IPSL, UPMC, CNRS, Paris, France

Abstract During the summer 2012, we carried out continuous measurements of the isotopic composition (δ) of water vapor over the near-surface subtropical North Atlantic Ocean (STRASSE cruise). In this region of excess evaporation, we investigate the control of evaporation and mixing with a lower troposphere-derived, isotopically depleted air mass on the near-surface δ. We use a simple model to simulate the near-surface δ as the result of a two end-member mixing of the evaporative flux with free tropospheric air. The evaporative flux δ was estimated by the Craig and Gordon equation while the δ of the lower troposphere was taken from the LMDZ-iso global atmospheric circulation model. This simulation considers instantaneous mixing of lower tropospheric air with the evaporated flux and neglects lateral advection. Despite these simplifications, the simulations allow to identify the controls on the near-surface δ. The d-excess variability is largely a consequence of varying kinetic effects during evaporation, even during a convection event when the input of tropospheric vapor was strong. Kinetic effects and mixing processes affect simultaneously the near-surface δ and result in the vapor occupying distinct domains in the δ^{18}O-δD space. The relative humidity-d-excess relationship shows that the closure assumption overestimates the d-excess variability at short time scales (less than a day). We interpret this as due to an effect of the residence time of the near-surface water vapor on the d-excess. Finally, we highlight the importance of reproducing mixing processes in models simulating isotopes over the subtropical North Atlantic Ocean and propose an extension of the closure assumption for use in initial conditions of distillation calculations.

1. Introduction

For more than 50 years, the isotope composition (δ) of water vapor has been used to investigate the hydrological cycle, providing key insights on modern and past climates [e.g., *Dansgaard et al*., 1984; *Vimeux et al*., 2001; *Johnsen et al*., 2001; *Lawrence et al*., 2004; *Kurita et al*., 2011; *Tremoy et al*., 2012]. The cornerstone of this approach is a robust understanding of the overall fractionation processes that control the δ of fluxes between the various compartments of the water cycle. Recently, laser spectrometry has allowed to continuously measure the δ of water vapor, providing an unprecedented opportunity to study isotopic effects in oceanic evaporation [*Benetti et al*., 2014; *Steen-Larsen et al*., 2014]. Here this technique is applied in the subtropical Eastern North Atlantic Ocean (ENAO), where high net evaporation occurs.

During oceanic evaporation, the δ of the evaporated flux (δ_e) is controlled by equilibrium and kinetic isotope effects [*Craig and Gordon*, 1965]. Equilibrium fractionation between liquid and vapor depends on sea surface temperature (SST), and the fractionation factor has been experimentally established by Majoube in 1971. Other studies have confirmed these estimates [*Horita and Wesolowski*, 1994; *Barkan and Luz*, 2005]. Kinetic fractionation takes place during the diffusion of water vapor across the thin diffusive boundary layer at the ocean surface because each isotopic molecule has a distinct molecular diffusivity in air [*Craig and Gordon*, 1965]. Diffusion, and the kinetic isotopic effect associated to it, is affected by relative humidity, wind speed (impacting on the relative proportion of vapor transport by turbulence or diffusion), and the δ of local moisture [*Craig and Gordon*, 1965; *Gat*, 1996]. A calculation of the kinetic fractionation factor based on the Brusaert model of evaporation has been carried out in 1979 by *Merlivat and Jouzel* [1979]. These authors suggest the existence of two fractionation regimes depending on wind speed: a wind speed of less (more) than 7 m s^{-1} corresponds to the smooth (rough) transport regime. The strongest (weakest) fractionation occurs during smooth (rough) regime.

©2015. American Geophysical Union. All Rights Reserved.

Understanding kinetic isotope effects during evaporation is crucial to interpret field observations and correctly implement isotopes in computer models of the water cycle. When considering kinetic isotope effects, the parameter of interest is the d-excess, as defined by Dansgaard in 1964: d-excess = $\delta D - 8 \times \delta^{18}O$. Between 20 and 30°C (including subtropical sea surface temperatures), the d-excess of the vapor is not affected by equilibrium fractionation and is a measure of the intensity of kinetic isotope effects. Strong kinetic isotope fractionation (e.g., low humidity and low wind speed) leads to high d-excess in the water vapor. To investigate kinetic processes during evaporation, we obtained a high-resolution record of the δ of water vapor over the subtropical ENAO, alongside with continuous records of the parameters that influence the strength of the evaporative flux (e.g., wind speed, sea surface temperature (SST), and specific humidity (q)) [*Benetti et al*., 2014]. Based on ERA-Interim (latest global atmospheric reanalysis produced by the European Centre for Medium-Range Weather Forecasts), the regional annual net divergence flux (E-P) was on the order of 1.3 m yr^{-1} in 2012 and indicates a strong contribution of evaporation at the ocean surface. For summer conditions, convection processes are uncommon and rarely affect the higher troposphere. Indeed, trade winds lead to a strong temperature inversion between the free troposphere and the marine boundary layer (MBL), and water vapor exchanges between the two layers are limited [*Albrecht*, 1989; *Chen and Feng*, 2001]. However, the humidity of the lower free troposphere (LT) (below 3–4 km) affects the MBL by sporadic entrainment of air from the LT into the MBL through the inversion layer. Thus, the subtropical ENAO is a key area for understanding how atmospheric vapor acquires its δ close to the evaporative source before being transported to other regions through the hydrological cycle.

In a first approach to interpreting this data set, *Benetti et al*. [2014] assumed that the water vapor at the surface of the subtropical ENAO originates only from evaporation. This assumption was made because the area is characterized by strong evaporation and limited vertical mixing with relatively dry tropospheric air (region dominated by large-scale subsidence of dry air). *Benetti et al*. [2014] show that d-excess is negatively correlated with relative humidity normalized to SST (RHS) ($r = 0.89$) and that this anticorrelation is well reproduced by the closure assumption, a mathematical relation that calculates surface vapor δ assuming that vapor originates only from evaporation (MJ79). This strong link between RHS and d-excess has been observed in other oceanic regions [*Gat et al*., 2003; *Uemura et al*., 2008; *Steen-Larsen et al*., 2014] and can be used to predict the d-excess of precipitation [*Pfahl and Sodemann*, 2014].

Contrary to the d-excess, the variability in δ values was not reproduced by the closure assumption that neglects mixing with tropospheric vapor ($r = 0.53$ for $\delta^{18}O$, $r = 0.02$ for δD). Clearly, mixing with other depleted air masses contributes, alongside kinetic effects, in controlling near-surface δ. This is not surprising because in cloud/condensation processes, Rayleigh distillation depletes the atmospheric water vapor mainly via equilibrium fractionation, affecting δ without changing the d-excess. Thus, in the trade winds, water vapor above the surface atmospheric layer may have d-excess similar to that of near-surface vapor but lower δ [*Benetti et al*., 2014]. *Jouzel and Koster* [1996] and *Kurita* [2013] show from models and observations that the use of the closure assumption overestimates near-surface δ in the subtropics. They explain this bias by the contribution of other (depleted) sources in addition to evaporation. Thus, in the present study, we release the closure assumption and investigate the relative contribution of evaporation and other depleted air masses in controlling the δ of water vapor at 17 m height. A short event of convection is also presented to illustrate the link between the water vapor δ and the spatial organization of the convection—this link has been previously investigated in detail over the tropical ocean by the study of *Lawrence et al*. [2004].

First, the controls on δ values above the ocean surface—specifically evaporation and mixing with a depleted air mass—is investigated in plots of the surface water vapor δ in the $\delta^{18}O$-δD and RHS-d-excess diagrams. Second, to understand if evaporation and mixing can quantitatively explain the observed isotopic variability at 17 m, we simulate the near-surface mixing between the evaporated vapor and a depleted air mass originating from the LT. In this approach, we consider that each level of the MBL is the result of instantaneous mixing of vapor from the LT and from the evaporated flux in a proportion that varies with height above the ocean (Figure 1). The limitations of our simplistic approach are discussed in section 5.2. The LT end-member characteristics are provided by an isotopic general circulation model (LMDZ-iso) and the δ of the evaporative flux (δ_e) is calculated with the *Craig and Gordon* [1965] equation. We validate the humidity of the LT provided by LMDZ-iso with radiosonde data collected during the cruise. Assuming that the q and δ values

©2015. American Geophysical Union. All Rights Reserved.

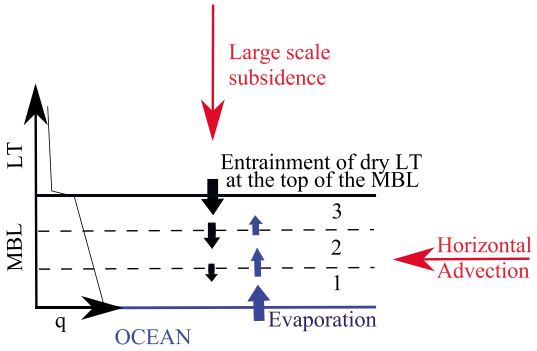

Figure 1. Schematic view of the mixing processes in the trade wind marine boundary layer of the North Atlantic. At each level, the water vapor content results from mixing in different proportions of water from evaporation and from the LT. The contribution of evaporation is the strongest in the layer 1. A supplementary source of water vapor comes from horizontal advection. The assumption made in our modeling approach is that the laterally advected air results from mixing processes between evaporated vapor and vapor from the LT that took place in adjacent regions. The schematic profile of the specific humidity (q) is also shown.

of both sources are known and that mixing is instantaneous, mixing proportions can be used to simulate water vapor δ values at 17 m ($\delta_{17\,m}$). Finally, we compare simulations and observations to understand the controls on vapor δ values above the subtropical ocean surface.

2. Methods

2.1. Isotope Measurements: Water Vapor and Seawater

The analytical procedure is briefly summarized here with a more detailed description provided in *Benetti et al.* [2014]. A laser analyzer Picarro L2130-I equipment was installed on the R/V *Thalassa* with air pumped at an altitude of 17 m above the sea surface. We followed the protocol elaborated by *Steen-Larsen et al.* [2013] to calibrate the measurement. We used three liquid standards with known δ to calibrate the data on the Vienna SMOW (VSMOW) scale ($\delta^{18}O_{VSMOW}$, δD_{VSMOW}; −0.56‰, −3.75‰; −6.60‰, −45.42‰; −15.81‰, −120.68‰). To correct instrumental drift, we injected the liquid standard with the closest δ value to the local vapor ($\delta^{18}O_{VSMOW}$, δD_{VSMOW}; −15.81‰, −120.68‰) at least twice a day. We estimated the concentration effect by injecting different amounts of liquid water into the vaporizer (two tests have been done in field conditions on 29 August and 13 September 2012). During the measurement, the instrumental accuracy of a 10 min average was 0.16‰ for $\delta^{18}O$, 0.4‰ for δD, and 1.4‰ for d-excess. Surface seawater was also regularly sampled to have a knowledge of the δ of source water for evaporation (at least once a day). Samples have been analyzed with the same Picarro used for the vapor measurement. The instrumental accuracy for liquid samples is 0.05‰ for $\delta^{18}O$ and 0.3‰ for δD.

2.2. Meteorological Measurements at 17 m

Standard atmospheric parameters were measured by a BATOS meteorological station from the French Met Office, located just above the position where the sampling of air for isotopic vapor measurement was installed. The station continuously measured air temperature (Ta), wind direction, wind speed, and relative humidity (RH). The RH was calibrated with a psychrometer. The largest difference between the two instruments was 2%. The specific humidity (q) was measured by the Picarro L2130-I and was calibrated by the humidity measured by the BATOS station. The correlation coefficient between the two measurements was 0.99. Sea surface temperature (SST) was continuously measured by a calibrated thermosalinograph at 3 m depth, and this provides an estimate of SST to within 0.2°C most of the time, except for a few midafternoon days with low winds.

2.3. Estimation of the Humidity and Isotope Composition of the LT

We used the atmospheric general circulation model LMDZ-iso to obtain an estimate of the q and the δ of the LT. LMDZ-iso is based on the LMDZ4 general circulation model [*Hourdin et al.*, 2006] and simulates water isotopes [*Risi et al.*, 2010a, 2010b]. The model is forced by monthly SST fields from the National Centers for Environmental Prediction reanalysis [*Kalnay et al.*, 1996], and horizontal winds are nudged toward European Centre for Medium-Range Weather Forecasts operational analyses [*Courtier et al.*, 1998]. The spatial resolution of LMDZ-iso is 3.75° in longitude and 2.5° in latitude. We chose the grid point (33.75°W; 26.62°N) at 790 hPa as reference level of the LT (above the boundary layer and corresponding to a height of about 2 km). To estimate the vertical variability of troposphere humidity and the stratification between the MBL and the free troposphere, radiosondes were launched twice a day, usually in the morning and the evening. To check the reliability of the humidity from the LMDZ-iso model, we compare it to that measured with radiosondes in section 3.2.

©2015. American Geophysical Union. All Rights Reserved.

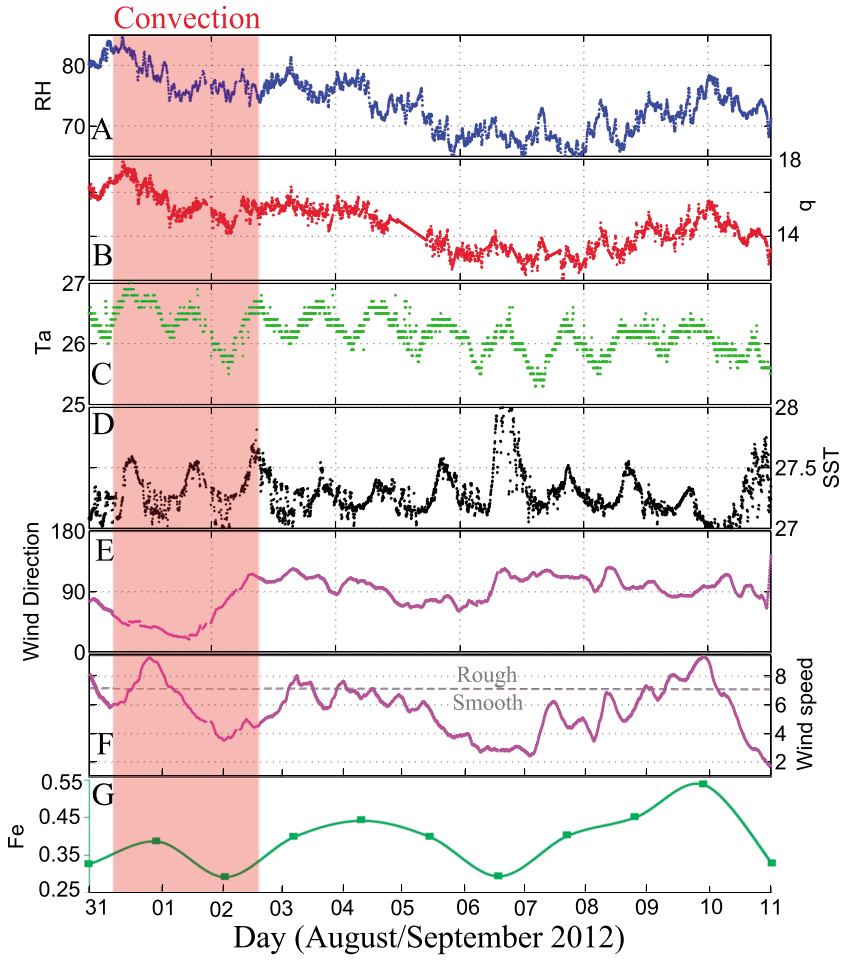

Figure 2. Time evolution of (a) relative humidity (%) (blue curve), (b) specific humidity (g/kg) (red curve), (c) Ta (°C) (green curve), (d) SST (°C) (black curve), (e) wind direction (0° for northerly winds), (f) wind speed (m s^{-1}), and (g) evaporated flux (cm/d) from 31 August to 11 September recorded during the STRASSE cruise. In Figure 2f, the grey-dashed line is 7 m s^{-1}. The red-colored period corresponds to the convection event.

3. Atmospheric Conditions

3.1. Meteorological Conditions

During the STRASSE cruise, the ship stayed close to 26°N and 35°W from 20 August to 11 September 2012. In this study, we consider only the second part of the cruise from 31 August to 11 September, which presents the largest variability in atmospheric conditions (Figure 2) and during which radiosondes have been launched. SST varied mostly between 27 and 28°C, and its variability has a negligible effect on the equilibrium fractionation factor between liquid and vapor [*Majoube*, 1971]. RH varied from 65 to 85% and *q* from 13.5 to 18 g kg^{-1}. Ta presents diurnal cycles with an amplitude of 1°C. The mean evaporated flux was on the order of 0.39 cm/d (based on the data collected on the R/V *Thalassa*, and applying COARE 5B algorithm) [*Fairall et al.*, 1996]. The mean wind speed at 10 m was 5.3 m s^{-1} with extreme values of 1.3 and 9.3 m s^{-1}. The wind speed was less than 7 m s^{-1} more than 80% of the time. The average of wind speeds larger than 7 m s^{-1} was only 7.8 m s^{-1}, therefore close to the transition between smooth and rough transport regimes (MJ79). Consistent with these wind speed conditions, we used the kinetic fractionation factor for the smooth air transport regime in the *Craig and Gordon* [1965] equation ($\alpha_k{}^{18}O = 1.006$ and $\alpha_k D = 1.0053$, MJ79). To complement this approach, we show in section 6 simulated results obtained imposing the rough regime for the two periods with the strongest winds (1 and 9 September, Figure 2f). The wind direction was mostly from the east indicating the dominance of trade winds, except around 1 September where the winds were northerlies. At this time, surface weather maps indicate that a low

©2015. American Geophysical Union. All Rights Reserved.

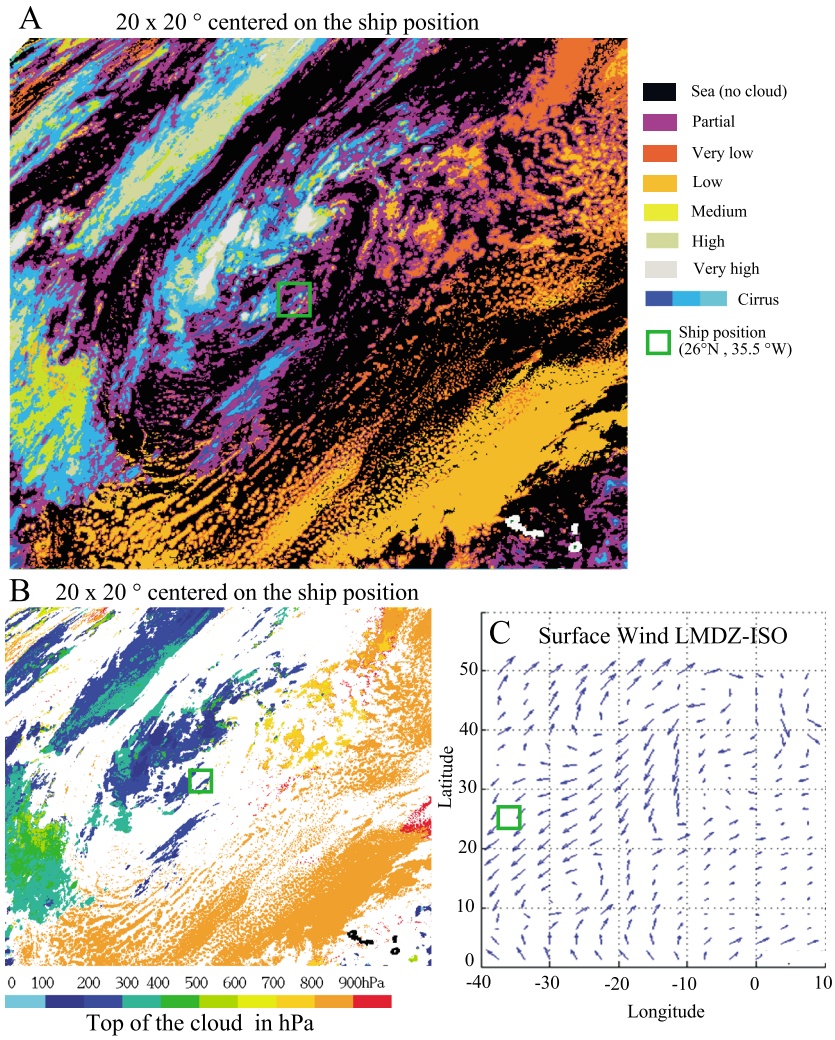

Figure 3. (a) Cloud classification. Grey and yellow indicates convection (cloud in the medium and high levels), orange and purple indicate a weak convection (partial cover or cloud only at low level), and black corresponds to the sea (no cloud). (b) Top of the clouds in hPa. No pressure is calculated for cloud partial cover. (c) Surface wind speed estimated by LMDZ-iso the 1 September (note that LMDZ-iso does not reproduce the observed convective event). The green square shows the ship position. The spatial scale is the same for Figures 3a and 3b: 20° × 20° centered on the ship position.

pressure passed southeast of the ship's position. During that day, cumulonimbus clouds were observed from the ship and a short evening event of rain (estimated to 2–3 mm rainfall) indicated convective processes. The period of moist convection is colored in red in Figure 2.

Figures 3a and 3b show a cloud-type map and a cloud top pressure (hPa) map during the moist convection period over a 20° × 20° domain centered on the ship's position. These maps are based on data from Spinning Enhanced Visible and Infrared Imager on board Meteosat Second Generation geostationary satellites (http://www.eumetsat.int/website/home/Satellites/index.html) processed with the Satellite Application Facility for NoWCasting algorithm developed by *Derrien and Le Glau* [2005]. A green square indicates the ship's position. The surface wind estimated by LMDZ-iso is also shown for 1 September (Figure 3c) (note that LMDZ-iso does not reproduce the convective event). The main characteristics of the moist convection event are the following: (1) The convective system was organized and not an isolated event, and (2) the ship was not at the center of the convective system but near its edge (the convective system passed to the north-west of the ship). (3) Close to the ship's position, the top of the cloud was at a pressure between 200 and 300 hPa—the convection was only moderate. (4) At the surface, the wind direction shows a cyclonic circulation to the southeast of the ship and thus displaced compared to the convective system at higher altitude.

©2015. American Geophysical Union. All Rights Reserved.

3.2. Vertical Humidity Structure of the LT and the MBL

The vertical profiles of specific humidity and virtual potential temperature are shown in Figure 4 (all available radiosoundings are shown). During our study period, the specific humidity (q) profiles show a dry troposphere and a humid MBL, except during the moist convection event when no stratification between layers is observed. Most of the time q is not homogeneous in the MBL, indicating ongoing entrainment of air from the LT into the MBL. The potential virtual temperature is used to estimate the stratification and the height of the MBL. During the more stable period after the convection event, the MBL seems well developed with a relatively strong separation between both layers. During this week, the MBL thickness varies from 1.5 to 2.5 km. In the following, we use these humidity profiles to check the reliability of the LT humidity simulated by LMDZ-iso.

Radiosoundings indicate a humidification of the LT due to a moist convection around 1 September (Figure 5a, red and black profiles). When the convection is most intense, q in the LT reaches 10 g/kg (Figure 5a, black profile). At this time, the profile of q shows no stratification up to 4 km between the LT and the MBL, indicating a mixing of the MBL with at least the LT. The LMDZ-iso model does not reproduce convection: no rainfall events and no humidification of the troposphere are simulated (humidity around 5–6 g/kg). Therefore, we decided to use radiosoundings to estimate the q of the LT during the convection event (dashed line in Figure 5c). A stronger stratification leading to a drier troposphere was present before and after this convective event (blue profile in Figure 5a).

From 3 to 8 September in the morning, the LT was relatively dry and there was a clear stratification between LT and MBL (blue profile in Figure 5b). These observations agree well with the weak LT humidity estimated by the LMDZ-iso model (blue shading in Figure 3c, LT humidity less than 5 g/kg). Then, profiles show a humidification of the LT between 2 and 3 km (red curve in Figure 5b) that reaches a maximum humidity in the evening of 9 September (black curve in Figure 5b). These profiles support the gradual humidification of the LT reproduced by LMDZ-iso model (green shading in Figure 3c, increasing q from 4 to 8.4 g/kg). No radiosondes have been launched after this period.

The mixing calculation also requires an estimation of δ_{LT}. In Figure 6, $\delta^{18}O$, δD, and d-excess of water vapor calculated by the LMDZ-iso model at 790 hPa are shown. $\delta^{18}O$ varies from -23.3 to -15.5‰, δD varies from -172 to -112‰, and the corresponding d-excess from to 12 to 15‰. We have no means to check this modeled δ with measurements and therefore have to consider a large uncertainty in δ_{LT}. In particular, during the convective event, which is not reproduced by LMDZ-iso model, δ_{LT} is likely to be affected by several processes such as vertical mixing by convective drafts, condensation in the convective updrafts, rainfall reevaporation, or diffusive exchanges in unsaturated downdrafts [*Risi et al.*, 2008].

4. The $\delta^{18}O$-δD and the RHS-d-Excess Diagrams at the Near Surface

In this section we use the $\delta^{18}O$-δD and the RHS-d-excess relationships to illustrate how mixing processes and kinetic effects control the isotopic properties of near-surface vapor. First, we describe how kinetic processes control the $\delta^{18}O$-δD and RHS-d-excess relationships; second, we consider mixing and its impact on these relationships.

4.1. Kinetic Processes

At the high-resolution time scale of the measurements (each point is the average of 10 min of measurements), the distribution in the $\delta^{18}O$-δD space is more complex than a simple linear mixing relation (largest panel in Figure 7). In Figure 7a, where all measurements between 2 and 11 September (except those acquired during convection) are shown, the different colors show distinct time periods, each one having a distinct $\delta^{18}O$-δD relationships. The colored data groups follow each other at a rate different from the diurnal cycle (from 1 day to 1.7 day) (see the color bar in Figure 7a). The average slope, humidity, and d-excess of each group are summarized in Table 1. Four groups (red, dark blue, cyan, and green) are particularly elongated and define a strong linear regression. The average q and RHS of groups decreases with decreasing $\delta^{18}O$ (from right to left, Figure 7b and Table 1), whereas the average d-excess of groups increases with decreasing $\delta^{18}O$ (Figure 7c and Table 1). For example, there is an average d-excess difference of 9‰ and an average RHS difference of 7.9% between the two extreme groups (red and dark blue). This $\delta^{18}O$-δD distribution illustrates the strong imprint of evaporation and its kinetic effects on near-surface vapor. The $\delta^{18}O$-δD

©2015. American Geophysical Union. All Rights Reserved.

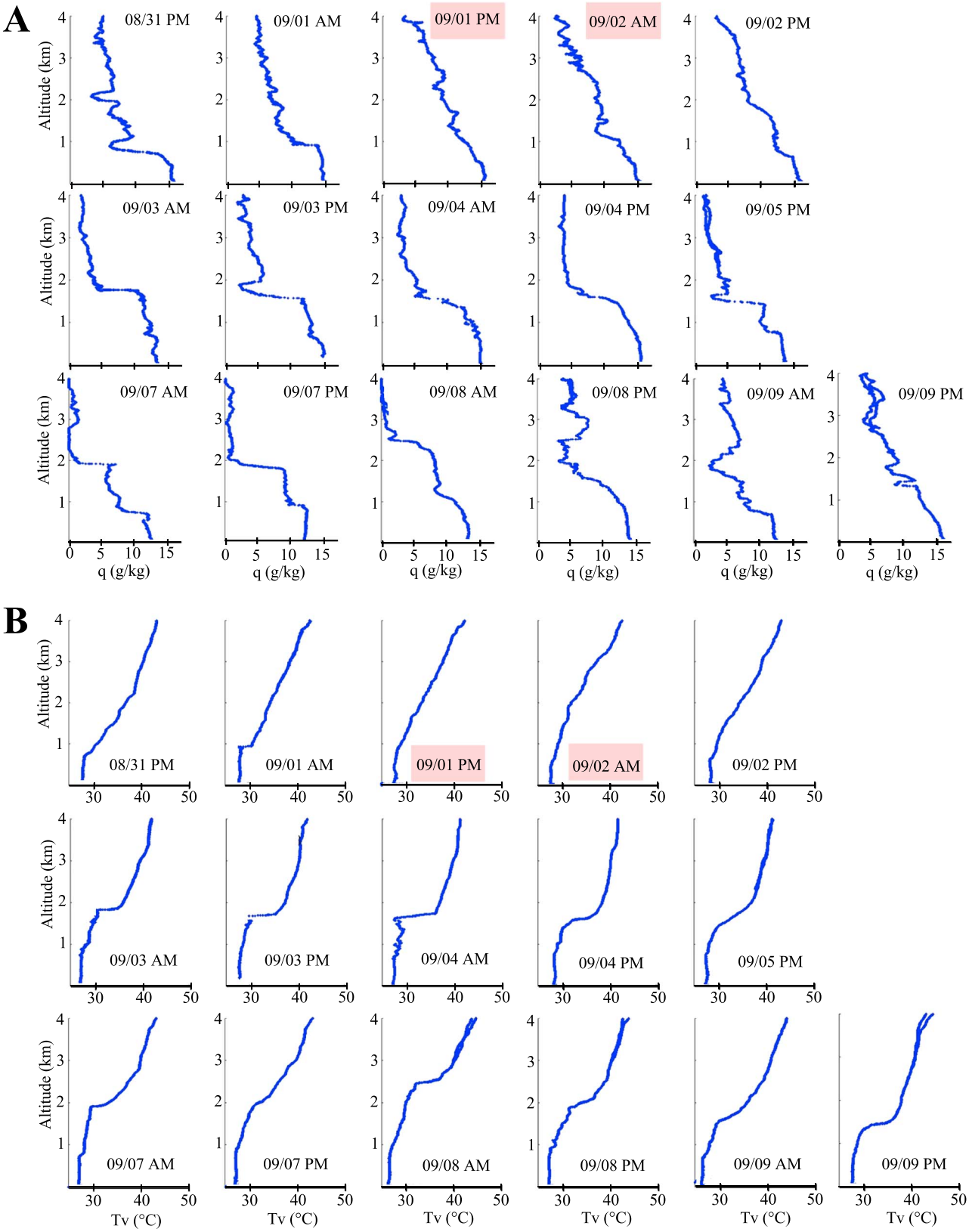

Figure 4. Vertical distribution of (a) specific humidity and (b) the potential virtual temperature from 31 August to 9 September 2012. All profiles available are shown. The date (mm/dd) is written on each plot. PM corresponds to approximately 8:00 P.M., and AM corresponds to approximately 8:00 A.M. The convection period is indicated in red.

©2015. American Geophysical Union. All Rights Reserved.

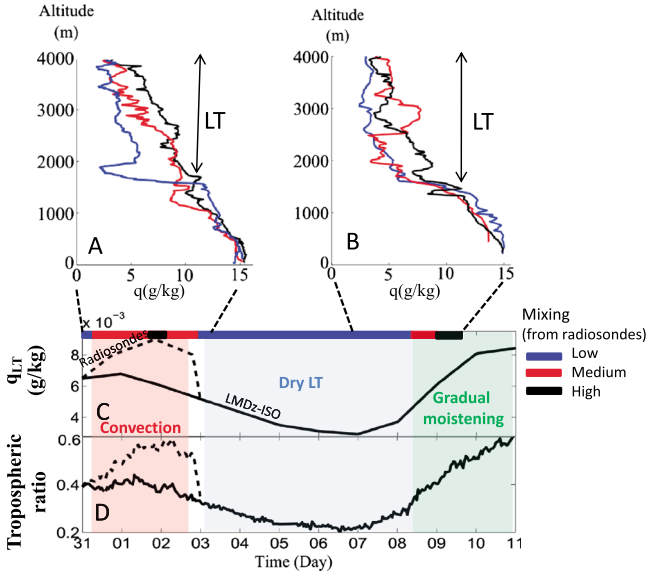

Figure 5. (a, b) Vertical profiles of specific humidity from the surface to 4 km. (c) Evolution of LT specific humidity from LMDZ-Iso (790 hPa). The dotted line represents the humidification due to the moist convection (from radiosondes). (d) Evolution of the tropospheric ratio ($= q_{LT} / q_{17\,m}$).

space shows that kinetic effects can lead to variation of around 1‰ in the near-surface vapor δ^{18}O during a week over the subtropical ENAO (see arrow in Figure 7a). Interestingly, we also found a clear imprint of kinetic effects in the more depleted water vapor during the convection event (Figures 7d–7f). During the convection period, two separate groups appear with slopes of 7.34 (pink group) and 7.62 (gray group). Consistent with our previous observations, the pink (grey) one is drier (more humid) and has higher (lower) d-excess (see average in Table 1).

Figure 8 presents the different groups in the RHS/d-excess diagram. This relationship has been already studied near the ocean surface by *Uemura et al.* [2008], *Gat et al.* [2003], *Benetti et al.* [2014], and *Steen-Larsen et al.* [2014]. Here we propose its investigation for shorter periods. The groups taken together follow the RHS/d-excess relationship estimated by the closure assumption. This observation is another way to show that the average d-excess of each group is controlled by kinetic processes during evaporation and confirm our previous comments on the δ^{18}O-δD space. The magenta and the orange group are characterized by a stronger slope within the RHS/d-excess relationship.

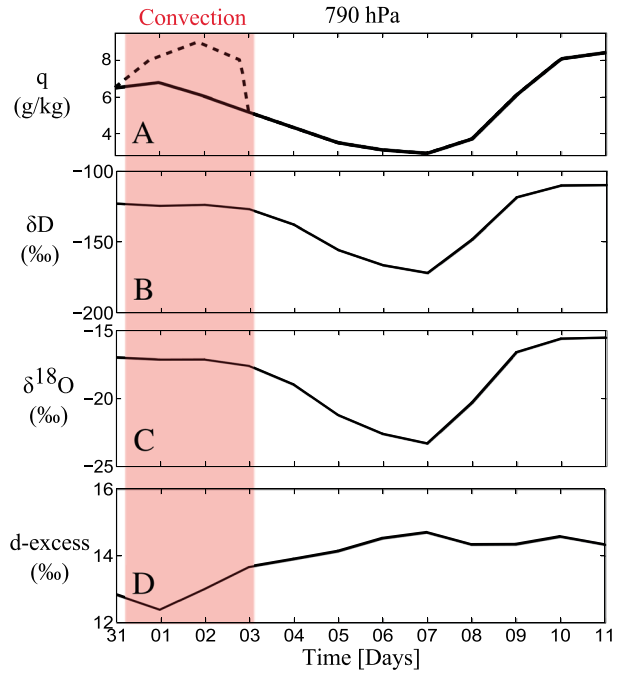

Figure 6. Characteristics of the LT at 790 hPa from LMDz-iso. Time evolution of (a) specific humidity (g/kg), (b) δD (‰), (c) δ18O (‰), and (d) d-excess (‰). The red-colored period corresponds to the convection event.

Large d-excess variation occurs in both groups with the strongest d-excess of the cruise (18‰) reached within the magenta group. During these two periods, we suggest that evaporation processes have a strong impact on the $q_{17\,m}$ variability. Furthermore, the slope in the δ^{18}O-δD space is 4 for the magenta group, which is consistent with a dominant role of kinetic effects in producing isotopic variations in this group (see next section).

4.2. Mixing Processes

In the previous section, we show that kinetic processes during evaporation produce distinct groups of vapor δ values in the δ^{18}O-δD and RHS/d-excess diagrams. In this section we focus on the processes controlling the δ variability within a group (thus on shorter time scales than those discussed in the previous section). In the four elongated groups (red, blue, cyan, and green), the slopes in the δ^{18}O-δD space vary from 5.5 to 6.7 (Table 1). These slopes are significantly lower than the slope of 8 which is generally observed in

©2015. American Geophysical Union. All Rights Reserved.

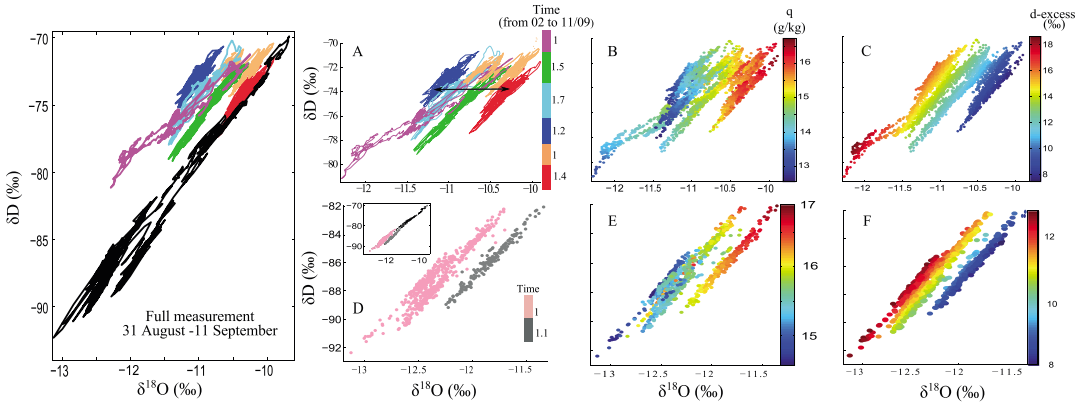

Figure 7. Water vapor isotope composition plotted on the δ^{18}O-δD space with colors corresponding to (a, d) time, (b, e) specific humidity, and (c, f) d-excess. Figures 7a–7c correspond to the more stable period after the convection event (from 2 to 11 September). In Figures 7a and 7d, the color bar indicates successive time periods while numbers indicate the length of the period in days. Figures 7d–7f are zooms for the period of isotopic depletion during the convection event. All measurements are shown together in the largest panel on the left where colors correspond to the time periods highlighted in Figure 7a for the more stable period while the complete convection period appears in black.

water vapor influenced by a Rayleigh distillation [*Craig*, 1961]. We interpret these slopes between 5.5 and 6.7 as due to mixing of vapor affected by an equilibrium Rayleigh distillation (slope approaching 8) with evaporated vapor having a much smaller slope due to kinetic effects (the theoretical slope produced uniquely by kinetic effects is equal to 0.88) [*Craig and Gordon*, 1965; *Gat*, 1996; *Araguás-Araguás et al.*, 2000]—clearly, the small slope values we observe reflect the proximity to the evaporative source. The largest slopes are observed during the convection event during which the inputs of LT vapor were strongest.

Information on mixing can also be extracted from data plots in the RHS/d-excess space. Within each of these four groups (red, blue, cyan, and green), important RHS variations occur (sometimes reaching 10%) with no associated strong variation in d-excess (only 2‰) (Figure 8). Based on the Craig and Gordon or on the closure equation, RHS variations of 10% should lead to d-excess variations larger than those observed within a group. Thus, on the time scale of a group, which lasts typically 1–2 days, the closure assumption overestimates the d-excess variability at 17 m—the slopes are significantly lower (see arrows in Figure 8). We suggest that mixing processes, which produce q and δ variations without significantly changing the d-excess at the near surface, also play an important role in defining the isotopic character of groups. At time scales shorter than a day, we expect that mixing influences near-surface vapor q and δ values nearly instantaneously, compared to variations in the evaporated flux.

In summary, we show that both the δ^{18}O/δD and RHS/d-excess relationships are helpful in deciphering the role of evaporation and mixing processes in controlling the near-surface δ. These plots show that at short time scales (approximately less than 1 day), mixing processes lead to a strong variation of humidity but limited d-excess excursions, while longer time scales are needed for changes in the isotopic properties of the evaporated flux to fully affect vapor near the surface. From the duration of each group, we suggest that 1 to 2 days could be necessary for the δ_e variability to fully affect the δ of the near-surface vapor. The duration of vapor renewal near the surface from evaporation in this region is in agreement with the study of *Bellon and Stevens* [2012] showing that 1 day is necessary for an increase of the evaporative flux to affect near-surface humidity in the trade wind MBL. Finally, it is important to keep in

Table 1. Characteristics of the Different Groups[a]

Group	Slope (R)	RH (%)	d-Excess	RHS (%)
1 (red)	6.74 (0.92)	76.4	8.6	70
2 (orange)	1.47 (0.48)	75.2	10.9	69
3 (dark blue)	5.77 (0.89)	68.5	15.2	61
4 (cyan)	6.06 (0.96)	68.6	13.7	62
5 (green)	6.19 (0.98)	73.8	11.6	67.39
6 (magenta)	4.03 (0.98)	73.55	14.60	65.5
7 (gray)	7.62 (0.98)	78.7	8.9	73
8 (pink)	7.34 (0.95)	75.9	11.5	69

[a]Same color as in Figures 7 and 8. RHS is the relative humidity with respect to the sea surface temperature.

©2015. American Geophysical Union. All Rights Reserved.

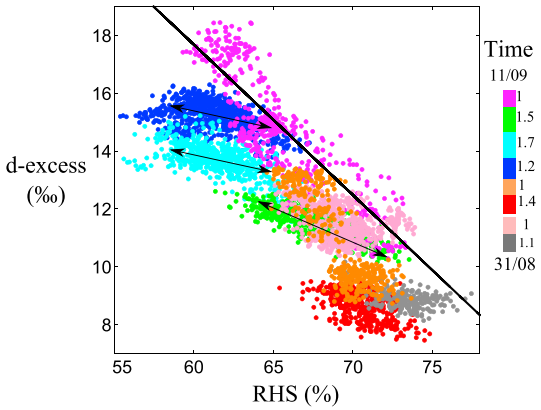

Figure 8. The RHS-d-excess relationship. The black line corresponds to the d-excess estimated by the closure assumption (MJ79). The color bar indicates the chronological order, and numbers indicate the length of the period in days.

mind that over the subtropical ocean, evaporation and mixing with the LT are not fully separable and impact together the near-surface δ.

5. The Modeling Approach

This section investigates the Keeling approach and proposes a simple mixing model to simulate isotope changes at the near surface and to attempt a quantitative evaluation of the mixing of LT vapor with evaporated vapor.

5.1. Evaluating Mixing Processes at the Near Surface

Figure 9 shows the δ measured at 17 m from 31 August to 11 September (including the convection event) ($\delta_{17\,m}$) (red dots), the δ_{LT} calculated by the LMDZ-iso model (black line), the δ of seawater (δ_{sw}) (dark blue dots), and the δ_E calculated using the *Craig and Gordon* [1965] equation (equation (1)). For this plot, we imposed our $\delta_{17\,m}$ measurements as near-surface δ values (δ_{ns}) in equation (1).

$$1+\delta_e = \frac{1}{\alpha_k}\times\frac{\alpha_{eq}^{vl}\times(1+\delta_{sw})-\mathrm{RHS}\times(1+\delta_{ns})}{1-\mathrm{RHS}} \quad (1)$$

where RHS is the relative humidity normalized to SST, α_{eq}^{vl} is the equilibrium fractionation factor between vapor and liquid, and α_k is the kinetic fractionation factor. In Figure 9, the vapor at 17 m lies close to a mixing line between the evaporated vapor and water vapor from depleted air masses which are consistent with the LT calculated by the LMDZ-iso model.

Mixing between two vapor sources produces a linear mixing line between δ and the inverse of q (Keeling plots) [e.g., *Keeling*, 1958; *Noone et al.*, 2011; *Tremoy et al.*, 2012; *Farlin et al.*, 2013]. Usually, the δ value of vapor sources is considered constant compared to the large range of δ variations in the vapor resulting from the mixing—in these conditions Keeling plots provide an efficient means to highlight mixing processes between two sources. In oceanic studies, when one of the two sources is the evaporative flux, Keeling plots provide specific information on the isotope composition of the evaporative flux [*Noone et al.*, 2011]. In short, when one source is the evaporative flux, the *Y* intercept of the Keeling plot corresponds to the δ value of the evaporative flux. In the following, we applied this two-source mixing approach to our near-surface measurement (Figure 10). The *Y* intercepts (*Y*) and determination coefficients (R^2) of the δ-1/q relationships for each previously identified group are presented in Table 2. Clearly, the *Y* intercepts do not provide a satisfactory estimate of the δ of the evaporative flux that has an isotopic composition between −9.27 and −7.52‰ for δ^{18}O and between −50.7 and −41.49‰ for δD. We also carried out Keeling plot on shorter time scales (from 10 min to 1 h), obtaining equally unsatisfactory results (not shown here).

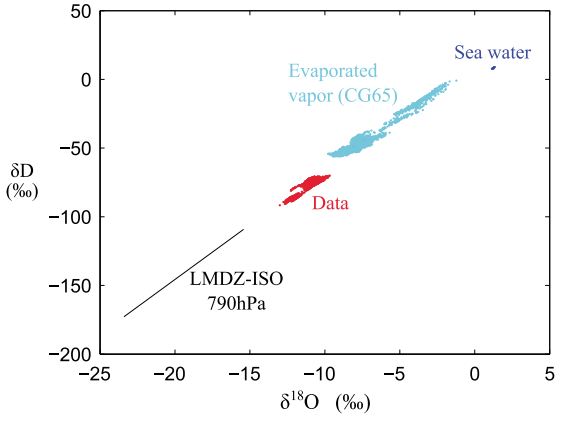

Figure 9. The marine evaporation process and the mixing with the lower troposphere in the subtropical region. The dark blue points correspond to surface seawater. The cyan blue points correspond to the evaporated flux. The red points correspond to the vapor measurement at 17 m. The dark line corresponds to the lower troposphere simulated by LMDZ-iso at 790 hPa.

In this oceanic study where mixing with depleted air masses is limited, the variability in δ_{17m} is small (in the order of 3‰ for δ^{18}O and 25‰ for δD)

©2015. American Geophysical Union. All Rights Reserved.

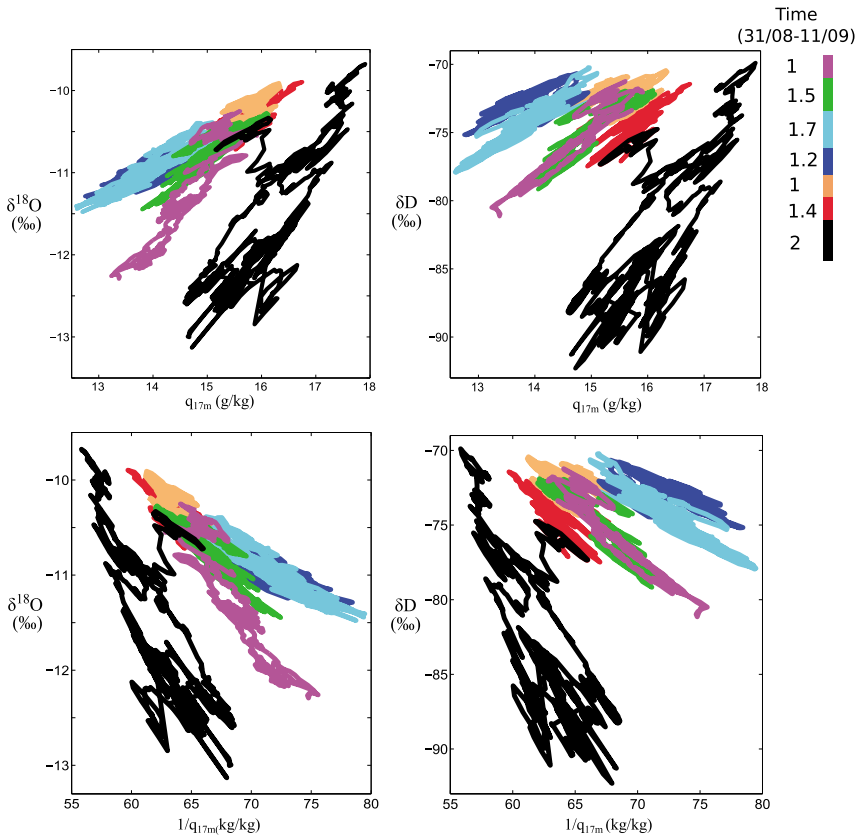

Figure 10. (a and b) δ-q relationships during the full measurement. (c and d) δ-$1/q$ relationships during the same period. The colors correspond to the groups defined in section 4. Y intercept and determination coefficient of the Keeling plots (Figures 10c and 10d) are presented in Table 2. The color bar indicates the chronological order, and numbers indicate the length of the period in days.

compared to those in the other continental or island studies previously cited. To our knowledge, the use of Keeling plots to explain such small isotopic variations in water vapor δ was never attempted. Here the linear regression through the vapor data is very sensitive to changes in the isotopic composition of the end-members. However, the variability of δ_e is larger than the variability resulting from the mixing (in the order of 10‰ for $\delta_e{}^{18}$O and from 50‰ for δ_eD) (see Figure 9). Furthermore, the isotopic composition of the depleted air mass contributing to the mixing can also evolve at short time scale. Thus, we suggest that in our particular field situation, Keeling plots are not applicable; this might well be the case also for other oceanic settings where the variability in δ values induced by mixing is relatively small. We therefore developed a simple modeling approach that considers instantaneous mixing between the two sources characterized by time-dependent humidity and δ values. This approach and its limitations are introduced in the next section.

Table 2. The Y Intercepts (Y) and Determination Coefficients of the Linear Regression of the $1/q$-δ Relationships (Keeling Plot) for Each Group (Ys and R^2s) and the Average δ^{18}O and δD of the Evaporative Flux Calculated With the *Craig and Gordon* [1965] Equation for the Different Groups (δ^{18}Oe and δDe)[a]

Group	Y (δ^{18}O)	Y (δD)	R^2 (δ^{18}O)	R^2 (δD)	δ^{18}Oe	δDe
1 (red)	−5.16	−44.43	0.43	0.26	−8.17	−44.30
2 (orange)	−2.88	−63.07	0.79	0.12	−8.40	−50.48
3 (dark blue)	−7.66	−55.81	0.64	0.40	−9.27	−54.38
4 (cyan)	−4.97	−36.8	0.87	0.84	−8.91	−50.68
5 (green)	−3.24	−28.8	0,84	0.88	−7.73	−46.27
6 (magenta)	−2	−19.31	0.84	0.90	−7.52	−41.49

[a]The colors correspond to Figure 10.

©2015. American Geophysical Union. All Rights Reserved.

5.2. Modeling Strategy: Scope and Limitations

To investigate the controls on vapor isotope characteristics of the full MBL, the minimal approach would imply a 1-D model covering the thickness of the MBL. As we do not have the information on the dynamics of the MBL needed to develop this 1-D model, we chose to limit our investigation to the controls on vapor dynamics and δ at the near surface (17 m), where our data were acquired. Here the modeling strategy considers that water vapor at 17 m results from a mixing between the evaporative source and another depleted air mass. An important issue is the choice of the humidity and isotope characters of the depleted air mass. As explained previously, this subtropical region is dominated by large-scale subsidence of dry tropospheric air—thus, a logical approach is to consider the LT as the isotopically depleted end-member of the mixing. In a simplified scheme (Figure 1), we consider that each level of the MBL is the result of mixing of vapor from the LT and from the evaporated flux in a proportion that varies with height above the ocean. Close to the ocean surface (level 1), the main water vapor source is evaporation, while at the top of the MBL (level 3), the main source is the LT. We use an estimate of LT characteristics provided by an isotopic general circulation model (LMDZ-iso), and the δ of the evaporative flux (δ_e) is calculated with the *Craig and Gordon* [1965] equation. Using q in the LT and at 17 m height, we derive mixing proportions of LT and evaporative water vapor that are representative of the near-surface vapor mixture. Simple mass balance considerations show that the proportion of water vapor from the LT incorporated in the vapor at 17 m (hereafter "tropospheric ratio") is equal to the LT to surface q ratio ($q_{LT}/q_{17\,m}$) (see calculation in Appendix A). We then use these mixing proportions to simulate $\delta_{17\,m}$. The vapor isotope composition at the near surface is calculated as

$$\delta_{17m} = (1 - r) \cdot \delta_e + r \cdot \delta_{LT} \tag{2}$$

where r is the tropospheric ratio (Figure 5d).

In this calculation, we took q_{LT} from the LMDZ-iso model except for the convective event where we impose the q measured with radiosondes (LMDZ-iso does not reproduce the convective event). Assuming that the tropospheric humidity is known to within (± 1 g kg^{-1}) results in an uncertainty of $\pm$ 5% on the tropospheric ratio. The δ_E term in equation (2) is the δ of the evaporation flux calculated with the *Craig and Gordon* [1965] equation (equation (1)). The CG65 model requires that δ is known at the near surface. Because in our modeling exercise $\delta_{17\,m}$ is the unknown, we combine equations (1) and (2) and solve the resulting expression for $\delta_{17\,m}$, obtaining an expression (equation (3)) that calculates the $\delta_{17\,m}$ as a function of known variables. Thus, equation (3) in an extension of the closure assumption that considers mixing with tropospheric vapor (the full derivation of equation (3) is described in Appendix B):

$$\delta_{17m} = \delta_{MJ79} \times (1 - b) + \delta_{LT} \times b \tag{3}$$

with $b = \frac{r \times \alpha_k \times (1 - RHS)}{(1 - r) \times RHS + \alpha_k \times (1 - RHS)}$ where δ_{MJ79} is the δ of the evaporated flux estimated by the closure assumption elaborated by MJ79 (the calculation of δ_{MJ79} is detailed in Appendix B) (a comparison to the closure assumption is carried out further below).

Because we derive r from q measurements at 17 m, this model captures much of the variability in isotope characteristics at 17 m. This is obviously limited in scope, but this modeling approach enables to run sensitivity tests that investigate the role of the different kinetic parameters and of mixing processes on the simulated vapor isotope characteristics at 17 m. A model not driven by humidity measurements would need to be driven by a high-resolution record of the dynamics of the near-surface atmosphere. This is clearly very difficult to obtain, and we chose to implement a model with less degrees of freedom that lends itself to the sensitivity analysis.

Before presenting results, we evaluate the limitations of this modeling strategy based on a simplified mixing process. First, this approach neglects horizontal advection. Nevertheless, we think that water vapor advected to the study area is a result of a previous vertical mixing between evaporation and LT water vapor, which happened in adjacent areas. For this reason, LT water vapor input does not come necessarily from the LT located just above the surface measurement. Thus, we will test the sensitivity of the simulated δ to the q and δ values of the LT by considering simulated LT characteristics from other subtropical LMDS-iso model grid points. Furthermore, water vapor from horizontal advection may experience different physical conditions along the way. However, at least on long (daily or longer) time scales, the region was rather homogeneous (both in SST, atmospheric temperature, and wind), and we assume that horizontal humidity gradient and isotopic changes associated with horizontal advection are small compared to those associated with vertical

©2015. American Geophysical Union. All Rights Reserved.

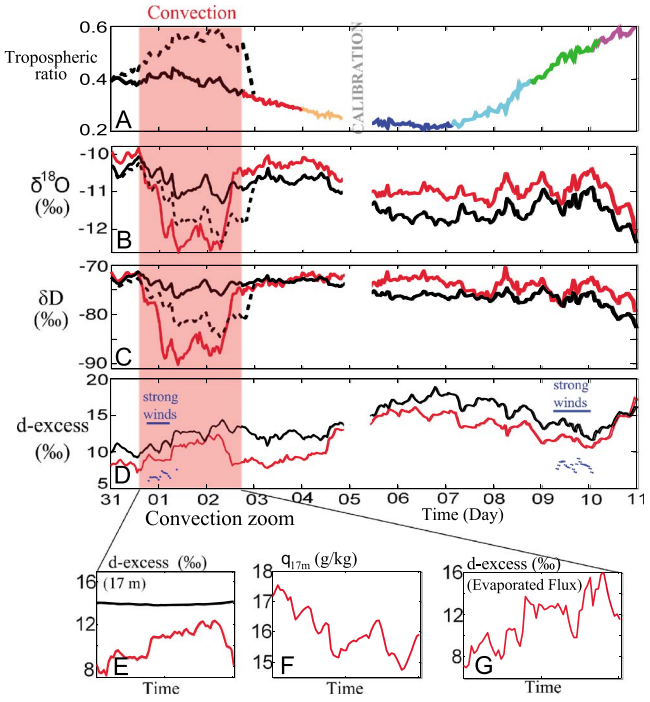

Figure 11. Time evolution of (a) tropospheric ratio(the different colors identify each group), (b) δ^{18}O (‰), (c) δD (‰), and (d) d-excess (‰); the blue points are d-excess estimated for the rough regime during periods of stronger winds. Red curves correspond to measurements, black curves to simulations (the dashed line uses the humidity estimated from radiosondes during the convection event). In Figure 11d, the two simulated curves are indistinguishable from each other. An enlargement of the convection period is shown: (e) d-excess at 17 m, (f) specific humidity at 17 m, and (g) d-excess of the evaporated flux. The black line in Figure 11e is the d-excess simulated with a constant d-excess in the evaporated flux.

mixing in this portion of the subtropical ocean. Nevertheless, the study from LMDZ-iso of the horizontal gradients of q and wind speed indicates that part of the variability of $q_{17\,m}$ is due to the advection of more humid air. We estimated the humidity horizontal gradient at 200 m from LMDZ-iso with the associated wind speed and found that lateral advection leads to an increase of q around 1.5 g/kg/d. The evaporation flux (average ≈0.39 cm/d, see Figure 2) leads to an increase of approximately 3.5 g/kg/d (considering a thickness of 1000 m), thus clearly more than the increase of q due to the horizontal advection. There can be also some phase changes along the way affecting isotopic composition, in particular when a perturbation favored for a short while deeper convection (while convection processes are rare in summer). The second limitation is that the hypothesis of instantaneous mixing does not consider the residence time of the water vapor in the MBL—this hypothesis implicitly assumes that the near-surface vapor is at steady state.

6. What Controls the Isotopic Properties of the Near-Surface Water Vapor?

During the whole study period, near-surface δ and d-excess estimated with the above procedure reproduce a large part of the variability observed in the measurements (Figures 11b–11d, red for data and black for model). The correlation coefficient is 0.74 for δ^{18}O, 0.76 for δD, and 0.90 for d-excess. The average difference between observation and calculation is 0.50‰ for δ^{18}O, 2.5‰ for δD, and 2.1‰ for d-excess. The largest differences for δ^{18}O and δD occur at the end of the convection event (1.4‰ for δ^{18}O and 10‰ for δD). As simulations agree reasonably well with observations, we use them to investigate processes controlling δ and d-excess at 17 m. This good agreement between data and simulations suggests also that assuming that the laterally advected air mass has undergone limited phase changes along the horizontal advection is a reasonable simplification in this situation of trade winds. In the following, we investigate the controls on the $\delta_{17\,m}$ in the different mixing regimes: (1) the convection event, when mixing with the troposphere is relatively intense, and (2) the period of stronger stratification between the MBL and the LT.

6.1. The Convection Event

During the convection event, from 31 August to the evening of 2 September, our data show a decrease of 2.5‰ (17‰) in δ^{18}O (δD) (see Figures 11b and 11c). The depletion can be in part due to in situ vertical mixing with the LT or to advection of air earlier depleted by vertical mixing. Whether this mixing happened during or before the convection event that we directly sampled would not modify, the following interpretations focused on the isotopic properties. During the convection event, the humidification of the troposphere produces an elevated tropospheric ratio (up to 60%) (see Figure 11a, black-dotted curve) and forces a decrease in $\delta_{17\,m}$ which approaches the measured values (see Figures 11b and 11c: dotted curve for estimation and red curve for data). Indeed, if the model is run imposing q_{LT} calculated by the LMDZ-iso model

©2015. American Geophysical Union. All Rights Reserved.

during the convective event, no significant δ decrease is observed (black continuous curve). As a result, the depleted $\delta_{17\,m}$ observed during the convection is due in part to the stronger input of depleted water vapor from the free troposphere into the MBL. These observations support the positive correlation between isotopic depletion and convective activity [e.g., *Dansgaard*, 1964; *Lawrence et al*., 2004; *Tremoy et al*., 2012]. We note that the depletion is stronger in the observations than in the box-model simulations. This could be because LMDZ-iso does not reproduce this convective event, there are large uncertainties in δ_{LT} during convection because this process can be associated with condensation, reevaporation of the rain, and diffusive exchanges between rain and vapor [*Risi et al*., 2008].

During the convection event, the measured d-excess increased by 4–5‰ (see Figure 11d, red curve). This increase is associated with a decrease larger than 2 g/kg in $q_{17\,m}$ (Figure 11f). The associated decrease in RHS leads to stronger kinetic isotope fractionation of the evaporative flux that could explain the d-excess increase. But at this time more than 50% of surface water vapor is derived from the LT, potentially affecting the d-excess. During the convection event, the increase in d-excess at 17 m is reproduced with or without considering the humidification of the troposphere (the curves are indistinguishable in Figure 11d). This suggests that the vapor from the LT brought during the convection event has little influence on near-surface d-excess. Furthermore, the decrease in RHS during convection leads to a strong increase in the d-excess of the evaporated flux (around 6‰, Figure 11g). If we impose a constant δ_e in equation (2), thus removing kinetic isotope effects, no increase of d-excess is produced at the surface (black curve in Figure 11e). These calculations suggest that, during the convection, the d-excess variability at 17 m is controlled by kinetic isotope effects during evaporation, rather than by the mixing with the troposphere.

Of course, there is a large uncertainty in the d-excess of the LT, because the LMDZ-iso model did not reproduce the convection. A likely explanation is that the near-surface drying due to increasing input of drier tropospheric air forced the d-excess of the evaporative flux to increase, influencing the d-excess signature at the near surface. This also explains why the closure assumption used in *Benetti et al*. [2014] reproduced the d-excess increase during this event of convection, even if the assumption of a single source of water vapor from evaporation has no reason to hold at this time of strong mixing. A similar conclusion was reached by *Risi et al*. [2010a, 2010b] who investigated the d-excess sensitivity to the convective activity within the MBL in the subtropics. These authors used a single-column model including a convective parameterization which considers convective subsidence and reevaporation of the rain. The simulations show that 55% of the MBL d-excess increase during convective activity is due to the decrease of RHS and its subsequent kinetic processes. This is smaller than what the data presented here suggest, a difference that could be attributed to the model results being characteristic of a larger boundary layer than the observations which are very close to the surface.

Within the limits of our data set, we explored the possible effect of the transport regime on the kinetic fractionation. For 12 h at the beginning of the convective period, the winds were stronger than 7 m s^{-1} (Figure 11d). For this period, we show in Figure 11d the d-excess estimated using the kinetic fractionation factor for the rough regime in the *Craig and Gordon* [1965] equation (blue points). This estimated d-excess is 5‰ lower than the one for the smooth regime. However, no such decrease in d-excess is observed. On 9 September, a new event of winds stronger than 7 m s^{-1} occurred, which did not lead to the expected change in d-excess. We point out that the period of strong winds was short (less than 1 day) and that the average of this strong wind speed was only slightly larger than the smooth-rough transition at 7 m s^{-1} (7.8 m s^{-1}): these are not the best conditions in which to test the effect of the wind transport regime on δ_e. Note that *Pfahl and Wernli* [2009] found by measuring 45 vapor samples from 2001 to 2006 in Israel that the best formulation of the kinetic fractionation factor which allows to fit the observations with the simulations is independent of the wind speed. Likewise, from vapor measurement in Bermuda Islands, *Steen-Larsen et al*. [2014] did not detect an effect of wind speed on the d-excess variability in the MBL. More measurements over the ocean are needed to clarify the role on the wind speed on the d-excess.

6.2. The Period After the Convection

In this section we focus on the period following the convection event characterized by a stronger stratification between the LT and the MBL, and we estimate separately the δ variability at 17 m due to mixing processes from that due to changes in the evaporated flux. At this time, vertical mixing is weaker and is mainly due to sporadic

©2015. American Geophysical Union. All Rights Reserved.

Table 3. Correlation Coefficient Between Observation and Simulation[a]

R	$\delta^{18}O$	δD
Standard (Local LT)	0.94	0.72
LT 1 (36.76°N, 33.75°W)	0.80	0.42
LT 2 (26.6°N, 26.25°W)	0.84	0.50
LT 3 (36.76°N, 26.25°W)	0.86	0.68

[a]Sensitivity of the simulated $\delta_{17\,m}$ to the q and δ values of the LT by considering simulated LT characteristics from three other subtropical model grid points.

entrainment of water vapor from the LT to the MBL. As explained previously, vertical mixing with the LT can happen further away and water vapor resulting from this mixing can be transported to the surface MBL of the study area by horizontal advection. For this reason, we test here the sensitivity of the simulated $\delta_{17\,m}$ to the q and δ values of the LT by considering simulated LT characteristics from three other subtropical model grid points: (1) north of the study area: 36.76°N, 33.75°W, (2) east of the study area: 26.6°N, 26.25°W, and (3) north-east of the study area: 36.76°N, 26.25°W. The results in Table 3 show that representing mixing processes by vertical mixing with the LT situated above the surface measurement reproduces best the variability observed at 17 m. To simplify the discussion, in the following, only the simulations using the LT situated above the study area are shown.

In Figure 12 we compare four other simulations with our measurements (red curve): (1) the standard simulation taking into account the q_{LT}, δ_{LT}, and δ_e variability (black), (2) a simulation forced with a constant δ_e to remove kinetic effects ($\delta^{18}O = -7.7‰$, $\delta D = -46.6‰$, average δ_e over the studied period, implemented by imposing a constant δ_e in equation (2)) (dark blue), (3) a simulation forced with a constant q_{LT} (4.8 g/kg, average over the studied period, implemented by imposing a constant q_{LT} in equation (3)) (magenta), and (4) a simulation forced with a constant δ_{LT} ($\delta^{18}O = -19.45‰$, $\delta D = -141.3‰$, average over the studied period, implemented by imposing a constant δ_{LT} in equation (3)) (green). The correlation coefficients between each simulation and the measurements are summarized in Table 4.

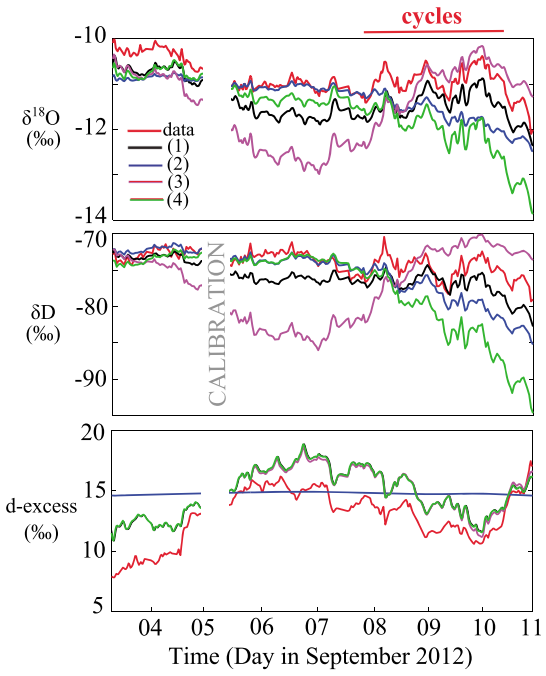

Figure 12. Evolution of δ and d-excess after the convection event. The red curve corresponds to the measurements and the black curve to the standard run (1). The dark blue curve corresponds to the simulation (2) (no variation of the evaporated flux isotopic composition), the magenta curve to simulation (3) (constant humidity of the LT), and the green curve to simulation (4) (constant δ of the LT). The black, magenta, and green curves are indistinguishable for the d-excess.

The correlation between the standard simulation and the measurements is strong for d-excess ($r = 0.86$). Simulations (3) and (4) show that the proportion of mixing with the LT and its d-excess variability does not affect the near-surface d-excess compared to the standard run (same correlation coefficients and curves indistinguishable in Figure 12). In addition, simulation (2) with constant δ_e does not reproduce the d-excess variability (the simulated d-excess variations due to mixing with the LT are less than 0.1‰). In summary, 74% of the d-excess variability is explained by the variability of δ_e, i.e., kinetic processes. Nevertheless, on the order of 25% of the variability is not reproduced in the standard run. More specifically, the d-excess variability is overestimated by the model. This could be due to natural variability of the LT d-excess that is not reproduced by the model, to nonstationarity effects or to horizontal inhomogeneity of water vapor properties near the ocean surface. As discussed in section 4.2, the overestimation of the d-excess variability is mainly because our model neglects the water vapor residence time at the surface.

The correlation between the standard simulation and the measurement is also very good for $\delta^{18}O$ ($r = 0.94$). Simulations (2)–(4) show that evaporation, mixing with the LT, and its δ variability are necessary to reproduce the $\delta^{18}O$ variability at 17 m (the correlation coefficients of the other runs are lower than those of the standard run). More precisely, q_{LT}

©2015. American Geophysical Union. All Rights Reserved.

Table 4. Correlation Coefficients Between Simulated Values and Measurements

R (Observation-Simulation)	d-Excess	$\delta^{18}O$	δD
Standard	0.86	0.94	0.72
Constant δ_e	0.67	0.53	0.71
Constant q_{LT}	0.85	0.48	−0.25
Constant δ_{LT}	0.86	0.61	0.69
LMDZ-iso	0.48	0.16	−0.27
Closure assumption (MJ79)	0.87	0.78	0.32

(controlling the tropospheric ratio) and the $\delta^{18}O$ of the evaporated flux are the most important parameters controlling the $\delta^{18}O$ variability at 17 m. These processes impact the near-surface $\delta^{18}O$ in the same direction and are together necessary to reproduce its variability. For example, three cyclic variations of $\delta^{18}O$ and q occurred between 8 and 10 September (see Figure 1 for q). These variations are well reproduced by the standard simulation but are underestimated in simulation (2) (which disregards kinetic effects). Thus, the two simulations indicate that these cyclic variations are the combined result of mixing with the LT and kinetic processes. Finally, simulation (4) suggests that the variability of $\delta^{18}O$ in the LT also contributes to the near-surface $\delta^{18}O$ variability.

The correlation between the standard simulation and the measurements is less good for δD ($r = 0.72$) than for $\delta^{18}O$ ($r = 0.94$) and d-excess ($r = 0.86$). Simulation (2) suggests that δD at 17 m is less impacted by δ_e variability than $\delta^{18}O$. The δ_{LT} seems to have no impact on δD at 17 m (simulation (4)). Finally, simulation (3) does not reproduce the observed variability ($r = -0.25$) and implies that the main process controlling δD at 17 m is the tropospheric ratio. In contrast to the d-excess and $\delta^{18}O$, δD is not affected much by evaporation processes and is the best indicator of mixing with the LT.

Contrary to δD, $\delta^{18}O$ variability is strongly affected by kinetic processes. Moreover, the variability of the δ_{LT} may also have an influence of $\delta_{17\,m}$, even if the simulations show that it is not the strongest control. Finally, the d-excess is the main indicator of evaporative conditions and is least impacted by mixing processes. The high correlation between observations and the standard run shows that q_{LT} variability simulated by LMDZ-iso is usually realistic (except during the convection event).

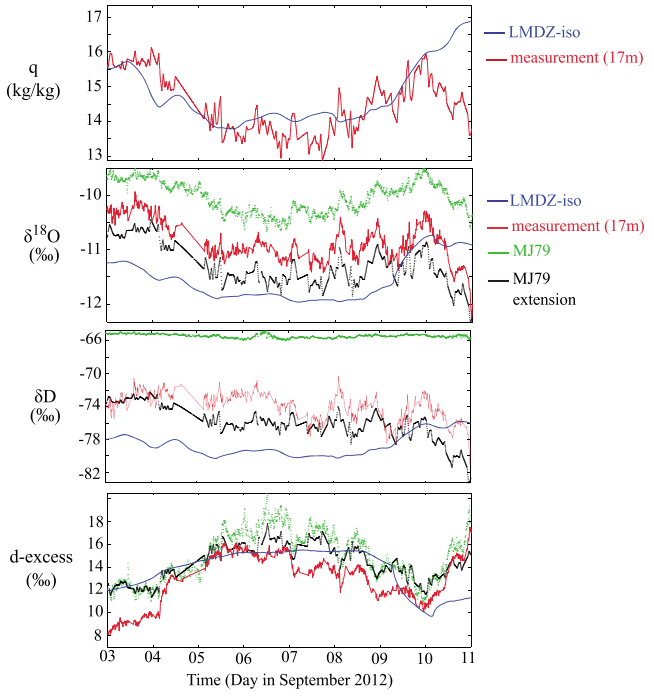

Figure 13. Time evolution of specific humidity, $\delta^{18}O$ (‰), δD (‰), and d-excess (‰) after the convection period. The red curve corresponds to the measurements and the black curve to the standard run; the dark blue curve to simulation at the surface from LMDZ-iso and the green curve to the estimation from the closure assumption (MJ79).

To place our findings in the broader context of modeling of vapor isotopes over the ocean, we compared in Figure 13 the simulation results with the near-surface δ estimated by LMDZ-iso between 0 and 36.6 m (between 1008.93 and 999.91 hPa) (blue curve), with the standard simulation (black curve) and with the measurements (red curve). The correlation coefficients between LMDZ-iso and the measurement are summarized in Table 4. The simple model simulation allows reproducing with much greater accuracy the $\delta_{17\,m}$ variability compared to the LMDZ-iso, especially at time scales shorter than a day, notwithstanding the fact that the general circulation model (GCM) considers many of the complex processes affecting near-surface δ which are not considered in our simple approach. According to our results, what matters the most is a good representation of the mixing between the evaporated flux and another depleted air mass, simplified here to the local LT.

©2015. American Geophysical Union. All Rights Reserved.

6.3. Comparison With the Closure Assumption and Importance of Mixing With the LT

The purpose of the MJ79 closure assumption is to provide a simple formula for the δ of near-surface vapor, which can then be used as initial conditions for distillation calculations [e.g., *Ciais and Jouzel*, 1994]. The closure assumption, however, overestimates near-surface δ over the subtropical ocean. *Kurita* [2013], for example, found from measurements over the subtropical Pacific Ocean that δD at the ocean surface was lower compared to the value estimated by the closure assumption; in addition, *Jouzel and Koster* [1996] compared δ at the near surface estimated by the closure assumption with δ estimated by GCMs in the subtropical region and showed also a positive bias in the closure assumption estimations compared to GCMs calculations. In our modeling exercise, δ estimated by the closure assumption is shown in Figure 13 (green curve). The closure assumption is poorly correlated with the δ measurement compared to our standard simulation that considers mixing with the LT (see Table 4). Our approach (see equation (3)) provides a valid alternative for estimating $\delta_{17\,m}$ over the subtropical ocean when mixing with the LT hinders the applicability of the closure assumption [*Jouzel and Koster*, 1996; *Delmotte et al*., 2000].

7. Conclusion

We have evaluated the role of mixing of LT moisture and the evaporated flux in controlling the near-surface water vapor δ and d-excess in the subtropical ENAO. The δ^{18}O-δD and RHS-d-excess relationships can be used to discriminate evaporation from mixing with the LT. They highlight the permanent coupling of the two processes and their role in controlling the humidity at the ocean surface. At time scales longer than a day, near-surface water vapor acquires different isotopic properties in response to the RHS variability at the surface and kinetic processes. However, we show that the closure assumption overestimates the observed d-excess variability at shorter time scales and we suggest that this is due to the role of the vapor time residence in controlling the d-excess variations at the near surface.

A simple mixing model in which the mixing is driven by high-frequency humidity measurements, reproduced a large part of the observed δ variability at the near surface. We show that 75% of d-excess variability is explained by kinetic processes during evaporation. Mixing with the LT has little impact on near-surface d-excess, even during an event of convection. Contrary to the conclusion for d-excess, we showed that correctly representing the mixing with the LT is critical to reproduce the near-surface vapor δ values. At the surface, δ^{18}O is more affected by kinetic processes than δD which is the best indicator of mixing with the LT. Further improvements would involve obtaining simultaneous measurement of δ^{18}O and δD in the free troposphere to have a better estimation of the LT variability and to investigate the impact of the δ variability of the LT on the near surface.

For future studies in which initial conditions for distillation calculations are needed, we suggest the use of an extended closure equation (equation (3)) when the atmospheric regime is similar. In practice, the difficulty in applying this extended closure assumption is to prescribe a δ value for the free-tropospheric water vapor. However, variations of this parameter were not the most crucial factor influencing $\delta_{17\,m}$ in a situation with trade winds. Finally, our study could help to evaluate the mixing between the surface and the LT in GCMs in which isotopes are implemented. Indeed, quantifying the vertical mixing between the MBL and the LT is crucial because this mixing strongly controls the climatic sensitivity of models [*Sherwood et al*., 2014].

Appendix A: Calculation of the Tropospheric Ratio

This annex presents the mass balance calculations showing that the tropospheric ratio is equal to the LT-to-surface specific humidity ratio ($q_{LT}/q_{17\,m}$).

The surface receives a vapor flux from evaporation of local seawater (F_{evap}) and exchanges vapor with the lower troposphere via incoming and outgoing air fluxes (F_{LT} and F_{out}) (Figure A1). To conserve the amount of air at the surface, the incoming and outgoing air fluxes are of equal magnitude and are referred to as F_{air} (in $m^3\,s^{-1}$):

$$F^{in}_{air} = F^{out}_{air} = F_{air} \quad \text{(A1)}$$

©2015. American Geophysical Union. All Rights Reserved.

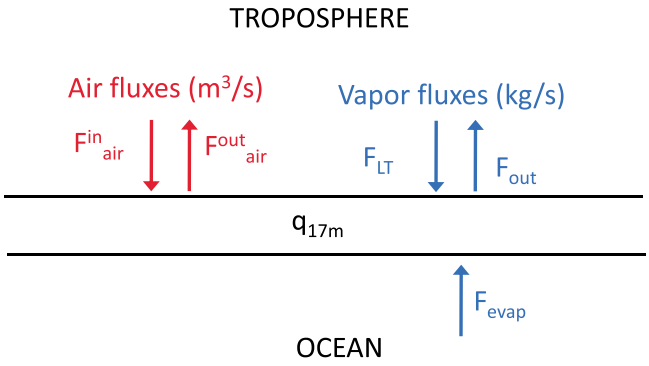

Figure A1. Simplified exchanges of air and vapor at 17 m height over the ocean considered in the present study. Red: exchange of air between the near-surface and the troposphere. Blue: incoming water vapor fluxes from the lower troposphere (F_{LT}) and from evaporation (F_{evap}), and outgoing vapor flux to the troposphere (F_{out}).

The evaporation flux, F_{evap}, is calculated with the bulk evaporation formula:

$$F_{evap} = \rho \cdot u \cdot CE_a \cdot (q_s - q_{17m}) \quad (A2)$$

where ρ is the density of air (in kg m^{-3}) at the near surface, calculated from the relative humidity, temperature, and atmospheric pressure measured at 17 m during the STRASSE cruise; u (in m s^{-1}) is wind speed; CE_a (set equal to 1.15×10^{-3}) is the dimensionless exchange coefficient; q_s (in kg kg^{-1}) is the saturation specific humidity at the near surface, and $q_{17\,m}$ (in kg kg^{-1}) is the specific humidity at 17 m height.

The vapor flux entering the surface from the troposphere, F_{LT} (in kg s^{-1}), is computed as follows:

$$F_{LT} = F_{air} \cdot q_{LT} \cdot \rho \quad (A3)$$

where q_{LT} (in kg kg^{-1}) is the specific humidity of the lower troposphere.

The vapor flux leaving the near surface for the troposphere is as follows:

$$F_{out} = F_{air} \cdot q_{17m} \cdot \rho \quad (A4)$$

An estimate of F_{air} is obtained by assuming steady state for total vapor at the surface:

$$O = F_{evap} + F_{LT} - F_{out} \quad (A5)$$

Substituting equations (A2), (A3), (A4) in equation (A5) and rearranging with respect to F_{air}, we obtain the following:

$$F_{air} = \frac{CE_\alpha \cdot (q_{17m} - q_s) \cdot u}{(q_{LT} - q_{17m})} \quad (A6)$$

In the study, we define the tropospheric ratio (r) by the proportion of water vapor from the LT incorporated at the near surface

$$r = \frac{F_{LT}}{F_{LT} + F_{evap}} \quad (A7)$$

By incorporating (A2), (A3), and (A6) in (A7) and after simplifications, we find that r is equal to the following:

$$r = \frac{q_{LT}}{q_{17m}} \quad (A8)$$

Appendix B: Extension of the Closure Assumption

This annex describes our derivation of the extension of the closure assumption. In our simulation, the isotopic ratio at the near surface (R_{ns}) is equal to the following:

$$R_{ns} = r \times R_{LT} + (1 - r) \times R_e \quad (B1)$$

where R_e is the isotopic ratio of the evaporated flux estimated by the Craig and Gordon equation:

$$R_e = \frac{\frac{R_{sw}}{\alpha^{lv}_{eq}} - RHS \times R_{ns}}{\alpha_k \times (1 - RHS)} \quad (B2)$$

where r is the tropospheric ratio (the proportion of water vapor from the LT incorporated into the near surface). R_{LT} and R_{SW} are, respectively, the isotopic ratios of the LT and the surface seawater. RHS is the relative

©2015. American Geophysical Union. All Rights Reserved.

humidity normalized to surface sea temperature. The equilibrium fractionation factor between liquid and vapor is α_{eq}^{lv}. The kinetic fractionation factor is α_k.

By combining (B1) and (B2), we obtain the following:

$$R_{ns} = \frac{\frac{(1-r)\times R_{sw}}{\alpha_{eq}^{lv}} + r\times\alpha_k\times(1-\mathrm{RHS})\times R_{LT}}{(1-r)\times\mathrm{RHS} + \alpha_k\times(1-\mathrm{RHS})} \tag{B3}$$

When $r=0$, we obtain the closure assumption:

$$R_{ns}(r=0) = R_{MJ79} = \frac{\frac{R_{sw}}{\alpha_{eq}^{lv}}}{\mathrm{RHS} + \alpha_k\times(1-\mathrm{RHS})} \tag{B4}$$

By reorganizing (B3), we obtain R_{ns} as a function of R_{MJ79}:

$$R_{ns} = R_{MJ79}\times(1-b) + R_{LT}\times b \tag{B5}$$

With $b = \frac{r\times\alpha_k\times(1-\mathrm{RHS})}{(1-r)\times\mathrm{RHS}+\alpha_k\times(1-\mathrm{RHS})}$

In the δ notation and considering a 17 m height for the near surface, (B5) is equivalent to the following:

$$\delta_{17m} = \delta_{m79}\times(1-b) + \delta_{LT}\times b \tag{B6}$$

Acknowledgments

We deeply thank three anonymous reviewers for their very useful comments that improved the quality of this paper. We are very thankful for precious advices and comments provided by Catherine Pierre, Liliane Merlivat, Françoise Vimeux, and Hans Christian Steen-Larsen. We also thank Aicha Naamar and Jerôme Demange for having shared their technical knowledge. LMDZ simulations were run on the Ada supercomputer at the IDRIS computing center. The Picarro equipment was purchased with support from different French institutions, in particular by IPSL, LOCEAN, LMD, and LATMOS. The STRASSE cruise on R/V *Thalassa* was supported by LEFE/INSU and TOSCA/CNES SMOS grants. We thank the crew and Genavir to have provided very good working conditions on this IFREMER research vessel. One can access the data used to produce the results of this paper by contacting Marion Benetti (marion.benetti@locean-ipsl.upmc.fr).

References

Albrecht, B. A. (1989), Aerosols, cloud microphysics, and fractional cloudiness, *Science*, *245*(4923), 1227–1230, doi:10.1126/science.245.4923.1227.

Araguás-Araguás, L., K. Froehlich, and K. Rozanski (2000), Deuterium and oxygen-18 isotope composition of precipitation and atmospheric moisture, *Hydrol. Process.*, *14*(8), 1341–1355, doi:10.1002/1099-1085(20000615)14:8<1341:AID-HYP983>3.0.CO;2-Z.

Barkan, E., and B. Luz (2005), High precision measurements of17O/16O and18O/16O ratios in H_2O, *Rapid Commun. Mass Spectrom.*, *19*(24), 3737–3742, doi:10.1002/rcm.2250.

Bellon, G., and B. Stevens (2012), Using the sensitivity of large-eddy simulations to evaluate atmospheric boundary layer models, *J. Atmos. Sci.*, *69*(5), 1582–1601, doi:10.1175/JAS-D-11-0160.1.

Benetti, M., G. Reverdin, C. Pierre, L. Merlivat, C. Risi, H. C. Steen-Larsen, and F. Vimeux (2014), Deuterium excess in marine water vapor: Dependency on relative humidity and surface wind speed during evaporation, *J. Geophys. Res. Atmos.*, *119*, 584–593, doi:10.1002/2013JD020535.

Chen, Y.-L., and J. Feng (2001), Numerical simulations of airflow and cloud distributions over the windward side of the island of Hawaii. Part I: The effects of trade wind inversion*, *Mon. Weather Rev.*, *129*(5), 1117–1134, doi:10.1175/1520-0493(2001)129<1117:NSOAAC>2.0.CO;2.

Ciais, P., and J. Jouzel (1994), Deuterium and oxygen 18 in precipitation: Isotopic model, including cloud processes, *J. Geophys. Res.*, *99*, 16,793–16,803, doi:10.1029/94JD00412.

Courtier, P., E. Andersson, W. Heckley, D. Vasiljevic, M. Hamrud, A. Hollingsworth, F. Rabier, M. Fisher, and J. Pailleux (1998), The ECMWF implementation of three-dimensional variational assimilation (3D-Var). I: Formulation, *Q. J. R. Meteorol. Soc.*, *124*(550), 1783–1807, doi:10.1002/qj.49712455002.

Craig, H. (1961), Isotopic variations in meteoric waters, *Science*, *133*(3465), 1702–1703.

Craig, H., and L. I. Gordon (1965), Deuterium and oxygen-18 variations in the ocean and the marine atmosphere, in *Proceedings of a Conference on Stable Isotopes in Oceanographic Studies and Paleotemperatures, Spoleto*, July 26–27, edited by E. Tongiorgi, pp. 9–130, Lab. of Geol. and Nucl. Sci., Pisa, Italy.

Dansgaard, W. (1964), Stable isotopes in precipitation, *Tellus*, *16*(4), 436–468, doi:10.1111/j.2153-3490.1964.tb00181.x.

Dansgaard, W., S. J. Johnsen, H. B. Clausen, D. Dahl-Jensen, N. Gundestrup, C. U. Hammer, and H. Oeschger (1984), North Atlantic climatic oscillations revealed by deep Greenland ice cores, in *Climate Processes and Climate Sensitivity*, *Geophys. Monogr. Ser.*, vol. 29, edited by J. E. Hansen and T. Takahashi, pp. 288–298, AGU, Washington, D. C.

Delmotte, M., V. Masson, J. Jouzel, and V. Morgan (2000), A seasonal deuterium excess signal at Law Dome, coastal eastern Antarctica: A Southern Ocean signature, *J. Geophys. Res.*, *105*(D6), 7187–7197, doi:10.1029/1999JD901085.

Derrien, M., and H. Le Glau (2005), MSG/SEVIRI cloud mask and type from SAFNWC, *Int. J. Remote Sens.*, *26*(21), 4707–4732, doi:10.1080/01431160500166128.

Fairall, C. W., E. F. Bradley, D. P. Rogers, J. B. Edson, and G. S. Young (1996), Bulk parameterization of air-sea fluxes for Tropical Ocean-Global Atmosphere Coupled-Ocean Atmosphere Response Experiment, *J. Geophys. Res.*, *101*(C2), 3747–3764, doi:10.1029/95JC03205.

Farlin, J., C.-T. Lai, and K. Yoshimura (2013), Influence of synoptic weather events on the isotopic composition of atmospheric moisture in a coastal city of the western United States, *Water Resour. Res.*, *49*, 3685–3696, doi:10.1002/wrcr.20305.

Gat, J. R. (1996), Oxygen and hydrogen isotopes in the hydrologic cycle, *Annu. Rev. Earth Planet. Sci.*, *24*(1), 225–262.

Gat, J. R., B. Klein, Y. Kushnir, W. Roether, H. Wernli, R. Yam, and A. Shemesh (2003), Isotope composition of air moisture over the Mediterranean Sea: An index of the air–sea interaction pattern, *Tellus B*, *55*(5), 953–965.

Horita, J., and D. J. Wesolowski (1994), Liquid–vapor fractionation of oxygen and hydrogen isotopes of water from the freezing to the critical temperature, *Geochim. Cosmochim. Acta*, *58*(16), 3425–3437, doi:10.1016/0016-7037(94)90096-5.

Hourdin, F., et al. (2006), The LMDZ4 general circulation model: Climate performance and sensitivity to parametrized physics with emphasis on tropical convection, *Clim. Dyn.*, *27*(7–8), 787–813, doi:10.1007/s00382-006-0158-0.

Johnsen, S. J., D. Dahl-Jensen, N. Gundestrup, J. P. Steffensen, H. B. Clausen, H. Miller, V. Masson-Delmotte, A. E. Sveinbjörnsdottir, and J. White (2001), Oxygen isotope and palaeotemperature records from six Greenland ice-core stations: Camp Century, Dye-3, GRIP, GISP2, Renland and NorthGRIP, *J. Quat. Sci.*, *16*(4), 299–307, doi:10.1002/jqs.622.

©2015. American Geophysical Union. All Rights Reserved.

Jouzel, J., and R. D. Koster (1996), A reconsideration of the initial conditions used for stable water isotope models, *J. Geophys. Res.*, *101*, 22,933–22,938, doi:10.1029/96JD02362.

Kalnay, E., et al. (1996), The NCEP/NCAR 40-year reanalysis project, *Bull. Am. Meteorol. Soc.*, *77*, 437–471, doi:10.1175/15200477(1996)077<0437:TNYRP>2.0.CO;2.

Keeling, C. D. (1958), The concentration and isotopic abundances of atmospheric carbon dioxide in rural areas, *Geochimica et Cosmochimica Acta*, *13*(4), 322–334.

Kurita, N. (2013), Water isotopic variability in response to mesoscale convective system over the tropical ocean, *J. Geophys. Res. Atmos.*, *118*, 10,376–10,390, doi:10.1002/jgrd.50754.

Kurita, N., D. Noone, C. Risi, G. A. Schmidt, H. Yamada, and K. Yoneyama (2011), Intraseasonal isotopic variation associated with the Madden-Julian Oscillation, *J. Geophys. Res.*, *116*, D24101, doi:10.1029/2010JD015209.

Lawrence, J. R., S. D. Gedzelman, D. Dexheimer, H.-K. Cho, G. D. Carrie, R. Gasparini, C. R. Anderson, K. P. Bowman, and M. I. Biggerstaff (2004), Stable isotopic composition of water vapor in the tropics, *J. Geophys. Res.*, *109*, D06115, doi:10.1029/2003JD004046.

Majoube, M. (1971), Fractionnement en oxygene-18 et en deuterium entre l'eau et sa vapeur, *J. Chim. Phys.*, *68*, 1423–1436.

Merlivat, L., and J. Jouzel (1979), Global climatic interpretation of the deuterium-oxygen 18 relationship for precipitation, *J. Geophys. Res.*, *84*(C8), 5029–5033, doi:10.1029/JC084iC08p05029.

Noone, D., et al. (2011), Properties of air mass mixing and humidity in the subtropics from measurements of the D/H isotope ratio of water vapor at the Mauna Loa Observatory, *J. Geophys. Res.*, *116*, D22113, doi:10.1029/2011JD015773.

Pfahl, S., and H. Sodemann (2014), What controls deuterium excess in global precipitation?, *Clim. Past*, *10*, 771–781, doi:10.5194/cp-10-771-2014.

Pfahl, S., and H. Wernli (2009), Lagrangian simulations of stable isotopes in water vapor: An evaluation of nonequilibrium fractionation in the Craig-Gordon model, *J. Geophys. Res.*, *114*, D20108, doi:10.1029/2009JD012054.

Risi, C., S. Bony, and F. Vimeux (2008), Influence of convective processes on the isotopic composition (δ^{18}O and δD) of precipitation and water vapor in the tropics: 2. Physical interpretation of the amount effect, *J. Geophys. Res.*, *113*, D19306, doi:10.1029/2008JD009943.

Risi, C., S. Bony, F. Vimeux, and J. Jouzel (2010a), Water-stable isotopes in the LMDZ4 general circulation model: Model evaluation for present-day and past climates and applications to climatic interpretations of tropical isotopic records, *J. Geophys. Res.*, *115*, D12118, doi:10.1029/2009JD013255.

Risi, C., A. Landais, S. Bony, J. Jouzel, V. Masson-Delmotte, and F. Vimeux (2010b), Understanding the ^{17}O excess glacial-interglacial variations in Vostok precipitation, *J. Geophys. Res.*, *115*, D10112, doi:10.1029/2008JD011535.

Sherwood, S. C., S. Bony, and J. L. Dufresne (2014), Spread in model climate sensitivity traced to atmospheric convective mixing, *Nature*, *505*(7481), 37–42.

Steen-Larsen, H. C., et al. (2013), Continuous monitoring of summer surface water vapor isotopic composition above the Greenland Ice Sheet, *Atmos. Chem. Phys.*, *13*(9), 4815.

Steen-Larsen, H. C., et al. (2014), Climatic controls on water vapor deuterium excess in the marine boundary layer of the North Atlantic based on 500 days of in situ, continuous measurements, *Atmos. Chem. Phys. Discuss.*, *14*, 2363–2401.

Tremoy, G., F. Vimeux, S. Mayaki, I. Souley, O. Cattani, C. Risi, G. Favreau, and M. Oi (2012), A 1-year long δ^{18}O record of water vapor in Niamey (Niger) reveals insightful atmospheric processes at different timescales, *Geophys. Res. Lett.*, *39*, L08805, doi:10.1029/2012GL051298.

Uemura, R., Y. Matsui, K. Yoshimura, H. Motoyama, and N. Yoshida (2008), Evidence of deuterium excess in water vapor as an indicator of ocean surface conditions, *J. Geophys. Res.*, *113*, D19114, doi:10.1029/2008JD010209.

Vimeux, F., V. Masson, G. Delaygue, J. Jouzel, J. R. Petit, and M. Stievenard (2001), A 420,000 year deuterium excess record from East Antarctica: Information on past changes in the origin of precipitation at Vostok, *J. Geophys. Res.*, *106*(D23), 31,863–31,873, doi:10.1029/2001JD900076.

©2015. American Geophysical Union. All Rights Reserved.